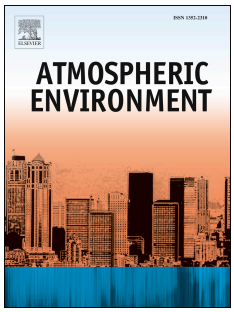

Observed dependence of surface ozone on increasing temperature in Shanghai, China

Yixuan Gu, Ke Li, Jianming Xu, Hong Liao, Guangqiang Zhou

PII: S1352-2310(19)30747-2

DOI: https://doi.org/10.1016/j.atmosenv.2019.117108

Reference: AEA 117108

To appear in: *Atmospheric Environment*

Received Date: 11 June 2019

Revised Date: 21 October 2019

Accepted Date: 1 November 2019

Please cite this article as: Gu, Y., Li, K., Xu, J., Liao, H., Zhou, G., Observed dependence of surface ozone on increasing temperature in Shanghai, China, *Atmospheric Environment* (2019), doi: https://doi.org/10.1016/j.atmosenv.2019.117108.

Observed dependence of surface ozone on increasing temperature in Shanghai, China

Yixuan Gu[a,b,*], Ke Li[c], Jianming Xu[a,b,*], Hong Liao[d], Guangqiang Zhou[a,b]

[a]Shanghai Typhoon Institute, Shanghai Meteorological Service, Shanghai 200030, China;

[b]Shanghai Key Laboratory of Meteorology and Health, Shanghai Meteorological Service, Shanghai 200030, China;

[c]John A. Paulson School of Engineering and Applied Sciences, Harvard University, Cambridge, MA 02138, USA;

[d]School of Environmental Science and Engineering, Nanjing University of Information Science and Technology, Nanjing 210044, China

*_Corresponding to_: Dr. Yixuan Gu (guyixuan@mail.iap.ac.cn) or Dr. Jianming Xu (metxujm@163.com)

Abstract. Eight-year measurements at urban (Xujiahui, XJH) and remote (Dongtan, DT) sites during time period 2010–2017 are employed to examine the surface ozone (O_3)-temperature relationship in Shanghai, China. O_3 pollution was getting worse in Shanghai, with daily maximum O_3 concentrations increasing at a rate of 2.47 ppb yr^{-1} in urban site. The climate penalty (m_{O3-T}), defined as the slope of O_3 change with increasing temperature, exhibited largest values in summer. Summertime O_3 increased faster as temperature increased, with mean rates of 6.65 and 13.68 ppb $°C^{-1}$, respectively in XJH and DT above 30°C. Sensitivity experiments indicate that the temperature dependence of biogenic volatile organic compounds (VOCs) emissions could be the main chemical driver of the high-temperature O_3 response in summer, since the simulated m_{O3-T} are most sensitive to changes of biogenic isoprene emissions. NO_x emission reductions strengthened the high-temperature O_3 response, with summer mean m_{O3-T} values increasing from 1.52 ppb$°C^{-1}$ during 2010–2012 to 2.97 ppb $°C^{-1}$ during 2013–2017. As NO_x emissions continue to decrease, the O_3 production in urban Shanghai tend to become transitional and the dependence of m_{O3-T} on the biogenic VOC emissions might be weakened. Model results suggest that anthropogenic VOC emission reductions would effectively relieve O_3 pollution and reduce the sensitivety of O_3 to increasing temperatures in urban Shanghai. Tailored emission reductions as well as scientific city planning strategies should be formulated to balance VOC/NO_x ratios, so as to wrestle with the challenges for future O_3 pollution under a warming climate.

Keywords: Ozone; isoprene; temperature; atmospheric chemistry; Shanghai

1. Introduction

Ground-level ozone (O_3) is a harmful photochemical pollutant threatening human health and land ecosystems (Sicard et al., 2013, 2016; Paoletti et al., 2014; Yue and Unger 2014; Feng et al., 2019; Li et al., 2019a). Surface O_3 is produced through complex and nonlinear photochemical oxidation of volatile organic compounds (VOCs) in the presence of nitrogen oxides ($NO_x \equiv NO+NO_2$) (Sillman, 2003). Despite the strict emission reductions conducted in past years, many megacities (e.g. Shanghai) in China are suffering from severe O_3 pollution in warm seasons (Geng et al., 2008; Tie et al., 2013; Wang et al., 2017; Li et al., 2019b). Episodes with daily maximum 8-h average (MDA8) O_3 larger than 70 ppb occur frequently in eastern China. The 4th highest MDA8 ozone value averaged over China is 86 ppb during 2013-2017, approximately 20−25% higher than the value over Europe and the United States (US) (Lu et al., 2018). Identifying drivers of high O_3 levels is therefore critical to understand the O_3 pollution in China.

Temperature has been reported to be a good predictor of high ground-level O_3, since it directly influences chemical kinetic rates and emission rates (e.g. biogenic VOCs) that are closely related to O_3 production (Jacob et al., 1993; Steiner et al., 2010). In addition, high temperature is usually associated with sunny, dry and stagnant atmospheric conditions which can further promote the accumulation of O_3 (Jacob et al., 1993; Jing et al., 2017; Li et al., 2019b). The climate change-driven warming is therefore expected to aggravate O_3 pollution and undermine the benefit of emission control measures (Liao et al., 2006; Jacob and Winner, 2009; Wang et al.,

2013; Fu et al., 2015). To illustrate the potential effect of climate change on surface O_3, the climate penalty factor is defined as the slope of the O_3 change with increasing temperature ($m_{O3\text{-}T}$, $\Delta O_3/\Delta T$) (Bloomer et al., 2009). The values of $m_{O3\text{-}T}$ were reported in the range of 2–8 ppb $°C^{-1}$ during ozone pollution seasons based on observational and numerical studies (e.g. Bloomer et al., 2009; Steiner et al., 2010; Rasmussen et al., 2012). Understanding how O_3 responds to temperature changes is considered to be helpful to evaluate the climate impact on air quality and develop effective emission-cutting policies to reduce O_3 pollution.

Several studies have attempted to examine drivers of the observed O_3-temperature relationship, suggesting that $m_{O3\text{-}T}$ is a function of multiple processes including peroxyacetyl nitrate (PAN) chemistry, biogenic VOC (BVOC) emissions, photochemical reactions, and temperature-related meteorological characteristics (Sillman and Samson, 1995; Steiner et al., 2010; Pusede et al., 2015; Shen et al., 2016). Based on observations and numerical experiments, Steiner et al. (2010) found that the decreases in PAN thermal decomposition and biogenic isoprene emissions at extremely high temperatures led to reductions in $m_{O3\text{-}T}$ at temperatures above approximately 39°C in California. By analyzing long-term ground-level measurements in the Midwestern US during 1990–2015, Jing et al. (2017) indicated that dry tropical weather could aggravate the ozone-climate penalty despite the NO_x emission reductions. Local VOC/NO_x ratios could greatly influence the response of $m_{O3\text{-}T}$ to emission reductions. For NO_x-limited areas, NO_x reductions could efficiently weaken $m_{O3\text{-}T}$ (Bloomer et al., 2009; Rasmussen et al., 2012; Pusede et al., 2014), while for

VOC-limited regions, O_3 concentrations and $m_{O3\text{-}T}$ could be more sensitive to changes in VOC emissions (Steiner et al., 2010). Thus, the high-temperature O_3 response and corresponding drivers should be carefully resolved under different emission circumstances.

Although studies have examined the impact of climate change on O_3 (Jacob and Winner, 2009; Steiner et al., 2010; Rasmussen et al.,2012; Jing et al., 2017), the high-temperature O_3 response was seldom evaluated observationally in Chinese megacities since O_3 has not been regularly monitored by environment agencies until 2013. Shanghai provides a typical locale to study the O_3-temperature relationship due to the early conducted O_3 measurements since 2005. What's more, as one of the largest megacities in China, Shanghai is home to a population of more than 20 million and is frequently engulfed by severe O_3 pollution episodes recently (Geng et al., 2008; Tie et al., 2009; Wang et al., 2017; Li et al., 2019b). The observed summer MDA8 O_3 increased by about 2 ppb yr^{-1} over Yangtze River Delta during 2013–2017 (Li et al., 2019b). The maximum 1-h O_3 concentrations could reach over 380 μg m^{-3} during polluted days in Shanghai (Shi et al., 2015). O_3 formation in urban Shanghai has been proved to be under VOC-limited regime that prevails in urban China (Geng et al., 2007; Ran et al., 2009; Tie et al., 2009). Long-term measurements suggested that O_3 concentrations increased by 67% in urban Shanghai from 2006–2015, which were mainly attributed to the reduction of the local NO_x emissions (Gao et al., 2017). Therefore, NO_x reduction measures together with the warmer climate might result in further increases in O_3 concentrations, leading to greater challenges for local O_3

pollution controls.

This work aims to identify the response of O_3 to the increasing temperatures and tease apart the corresponding temperature-driven chemical and meteorological reasons. We focus on Shanghai, since the city is still going through increasing high-O_3 episodes though strict emission reductions are conducted (Gao et al., 2017; Wang et al., 2017). Analysis is based on 8-year surface observations as well as simulations using the National Center for Atmospheric Research (NCAR) Master Mechanism model in Xujiahui (XJH, urban) and Dongtan (DT, rural) sites in Shanghai. The research results will provide important implications for how O_3 pollution responds to warmer temperatures and help to guide scientific emission control strategies for megacities in China.

2 Material and methods

2.1 Observational data

The measurements of O_3, NO_x, VOCs, as well as meteorological parameters (temperature, precipitation and wind speed) in this study are obtained from routine observations conducted by the Yangtze River Delta Center for Environmental Meteorology Prediction and Warning in Shanghai. Measurements from two sites are analyzed to represent the urban and rural conditions, including an urban-center site (XJH) greatly influenced by anthropogenic emissions and a background site (DT) located at the east edge of the city along the coast of the East Sea. The DT site locates near the nature reserve of the Chongming Island, with large sources of BVOCs generated from the forest. Hourly data collected from January 2010 to

December 2017, a period with available O_3 measurements in both sites, are used in this study. O_3 concentrations were measured with an analyzer from Ecotech, Australia (Model EC9810), which combined microprocessor control with ultraviolet photometry. NO and NO_2 concentrations were measured with a chemiluminescent trace level analyzer (TEI; Model 42iTL), with a detection limit of 0.025 ppb. The XJH site was equipped with additional instruments (a silonite canister with silonite coated valve, model 29-10622) for inconsecutive VOCs measurements in the morning (6–8 a.m.) during 2010–2015. The collected VOC samples include major atmospheric hydrocarbon compounds (e.g. alkane, alkene, and aromatic species) in Shanghai. More detailed information of VOC species, observation instruments, and methods can be found in Geng et al., (2009) and Gao et al. (2017).

2.2 Assessing trends of gases and temperature

The means of daily extremum concentrations of O_3, NO, and NO_2 of each year are used to analyze their year-to-year changes during time period 2010–2017. O_3 exceedance is yearly calculated to analyze changes in O_3 air quality during 2010–2017, which is the number of days with O_3 concentration exceeding the Chinese Grade II national air quality standard, namely MDA8 O_3 larger than 160 μg m^{-3}. The means of daily maximum and minimum temperature of each year are used to to analyze the temperature changes from 2010 to 2017. Two non-parametric methods were used to assess the trends of varables. The Mann-Kendall (MK) trend test (Mann 1945, Kendall 1975, Gilbert 1987) is used to examine the trend significance and the Sen trend estimate method (Sen, 1968) is used to estimate the slope of trend, which

could also be considered as the changing rate, during the studied period. Compared to the parametric methods which require data to be independent and normally distributed, the non-parametric trend test methods only need the data be independent and been widely used in the detection of trends of meteorological variables (Gocic and Trajkovic, 2013).

2.3 Determining the O_3-temperature relationship

The ozone-climate penalty factor ($m_{O3\text{-}T}$) is assessed to examine the dependence of surface O_3 on the increasing temperatures. The $m_{O3\text{-}T}$ is analyzed by fitting the relationship between daily maximum O_3 concentrations ($O_{3\text{-}max}$) and daily maximum temperature (T_{max}) by a second-order regression according to Bloomfield et al. (1996) and Jing et al. (2017). The regression equation can be expressed as $[O_{3\text{-}max}]=b_0+b_1[T_{max}]+b_2[T_{max}]^2$, where the value of $b_1/(-2b_2)$ reflects the temperature above which O_3 begins to increase as temperature goes up, and the value of $2b_2$ (ppb °C $^{-2}$) refers to the change rate of $m_{O3\text{-}T}$ with increasing temperature. Using this method, the slope of the O_3-temperature relationship ($m_{O3\text{-}T}$) becomes a temperature-dependent variable rather than a constant, which helps to identify its response on the increasing temperatures. To make comparisons with the $m_{O3\text{-}T}$ in summer (June–August), the regression is also performed for other seasons.

2.4 Chemical box model description

To examine the sensitivity of $m_{O3\text{-}T}$ to changes in precursors and emissions, numerical experiments are conducted using the NCAR Master Mechanism model (v2.5, https://www2.acom.ucar.edu/modeling/ncar-master-mechanism). The model is a

chemistry box model including approximately 5000 reactions among 2000 chemical species (Madronich and Calvert, 1990). The time-dependent chemical evolution of an air parcel can be calculated with known initial compositions, emissions and meteorological conditions, offering an opportunity to examine detailed chemical transformations for a single grid cell at a level that would be hard to achieve for 3-D models. The model used in this study is specified to consider major species involved in the urban O_3 chemistry, including NO_x, carbon monoxide (CO) and more than 32 VOC species. The photolysis rate is calculated on-line using radiative transfer code (TUV) as described in Madronich and Flocke (1999).

The initial concentrations of species are assigned according to the mean concentrations from measurements in this study and from Geng et al. (2007) and Zhang et al. (2012). The assigned diurnal variations of the planetary boundary layer height (PBLH) obtained from daily calculation of the Regional Atmospheric Environmental Modeling System for eastern China (RAEMS, Zhou et al., 2017). Anthropogenic emissions (Fig. S1) are based on the multi-resolution emission inventory for China (MEIC inventory, http://www.meicmodel.org/; Li et al., 2014) for year 2010. Biogenic isoprene emission rates are based on the isoprene-temperature parameterization of Guenther et al. (2006) (Fig. S2).

3. Results

3.1 Changes of ozone air quality in Shanghai during time period 2010–2017

Fig. 1 shows the year-to-year changes of O_3 exceedance, means of daily extremum O_3 concentrations and temperature in urban (XJH) and rural (DT) sites, respectively.

In general, all the variables exhibited increasing trends during time period 2010–2017, and the majority of the trends were significant at the 5% significance level. The number of O_3 exceedance days increased by 8.3 and 1.3 times from 2010 to 2017 in XJH and DT, respectively, indicating a worsening O_3 pollution environment in Shanghai. For urban site (XJH), the daily maximum and minimum 1-h O_3 concentrations ($O_{3\text{-max}}$ and $O_{3\text{-min}}$) increased at rates of 2.47 ppb yr^{-1}, and 1.18 ppb yr^{-1}, respectively, much faster than those in DT (1.19 ppb yr^{-1} for $O_{3\text{-max}}$, and 0.42 ppb yr^{-1} for $O_{3\text{-min}}$).

Fig. 2 displays the year-to-year variations of NO_x. In urban site (XJH), the observed means of daily maximum NO (NO_{max}) and NO_2 ($NO_{2\text{-max}}$) both exhibited significant decreases by -2.27 and -1.34 ppb yr^{-1}, respectivly, as a result of the NO_x emission reductions since the release of the China's 'Twelfth Five-Year' Plan for environmental protection in 2011. At the same time, the observed means of daily minimum NO (NO_{min}) and NO_2 ($NO_{2\text{-min}}$) exhibited opposite changes in XJH, with changing rates of +0.19 and -0.39 ppb yr^{-1}, respectively. For the background site (DT), the observed year-to-year variations of NO_x were much smaller than those in the urban site for the lower anthropogenic emissions. The O_3 concentrations there are less sensitive to the changes of anthropogenic emissions, exhibiting slower increasing rates than those in XJH. Observational and modeling studies have proved that rural sites in Shanghai are influenced by air masses with more aged pollutants, leading to less ozone depression and higher O_3 level than in the urban city (Geng et al., 2007, 2008; Shan et al., 2010, 2016).

After eliminating the effect of long-range transport, solar radiation, and VOC species, Gao et al. (2017) suggested that the rapid O_3 increase in Shanghai was mainly due to the changes of NO_x concentration. The calculated correlation coefficient (R) values are provided in Table S1. The R values was -0.80 between $O_{3\text{-max}}$ and NO_{max}, and -0.82 between $O_{3\text{-max}}$ and $NO_{2\text{-max}}$ XJH, indicating a strong depression of NO_x on O_3 at urban site. In addition, The increases in O_3 will very likely be further aggravated by warmer temperature, since the measured $O_{3\text{-max}}$ showed strong positive correlations with T_{max} in both XJH and DT, with R values of 0.62 and 0.87, respectively, during time period 2010–2017. Clarifying O_3 response to the increasing temperature and examining its drivers would be crucial to guild future emission-control policy making for megacities in China.

3.2 Observed relationship between ozone and temperature in Shanghai

Fig. 3 displays the observed O_3-temperature relationship in Shanghai during 2010–2017, separated by seasons and sites. The statistical results of the second-order regression, as described in Sec. 2.3, are displayed in Table 1. Most of the time, $O_{3\text{-max}}$ increased as temperature went up. The $2b_2$ values were close to zero in spring, autumn and winter, suggesting that $O_{3\text{-max}}$ changes approximately linearly as T_{max} increases. In summer, $m_{O3\text{-}T}$ increased as temperature increased, with increasing rates($2b_2$) of 0.62 ppb $°C^{-2}$ in XJH and 1.34 ppb $°C^{-2}$ in DT. Observed $m_{O3\text{-}T}$ exhibited most significant increases at temperature above 30°C in summer, with mean values of 6.65 and 13.68 ppb $°C^{-1}$ in XJH and DT, respectively. The observed summertime temperature dependence of $m_{O3\text{-}T}$ exhibited larger values in rural site than in urban

site in Shanghai, which are quite different from those reported in Jing et al. (2017) with increasing rates ranging from 0.12–0.27 ppb $°C^{-2}$ in urban sites and 0.09–0.14 ppb $°C^{-2}$ in rural sites during 2008–2015 in US. The differences between the two regions could be largely attributed the different O_3 production regime. Since surface O_3 production were NO_x-limited in most sites reported in Jing et al. (2017), O_3 production was more sensitive to NO_x instead of VOCs.

Compared to those reported in studies from the US and Europe (e.g. Bloomer et al., 2009; Steiner et al., 2006, 2010), the observed O_3 changes and the O_3-temperature relationship in Shanghai exhibited distinct regional characteristics (Figs. 1–3). First, although strict NO_x emission control measures have been conducted, the observed $NO_{2\text{-max}}$ concentrations of approximately 40 ppb in urban Shanghai were still 2 times higher than those in US. (Jing et al., 2017). Secondly, the strong VOC-sensitive O_3 production regime in Shanghai resulted in different high-temperature O_3 response in urban and rural areas. Observed values of $m_{O3\text{-}T}$ in rural site are much larger than those in urban site, which is different from the findings in Sillman and Samson (1995) and Jing et al. (2017) who reported that rural sites with low NO_x emissions had smaller $m_{O3\text{-}T}$ than urban sites in the NO_x-limited regions. Therefore, it is very essential to identify the local drivers of the high-temperature O_3 response in Shanghai, especially in summer when O_3 concentrations exhibit the fastest increase with the increasing temperatures.

3.3 Factors driving $m_{O3\text{-}T}$ in Shanghai

3.3.1 Observed precursors and their relationships with temperature in summer

256 The responses of O_3 precursors to increasing temperature were usually considered to
257 be extremely important in determining the O_3 climate penalty (e.g. Bloomer et al.,
258 2009; Steiner et al., 2010). To evaluate the changes in O_3 precursors and their
259 impacts on $m_{O3\text{-}T}$, observed seasonal variations of isoprene and NO_x, as well as their
260 relationships with temperature in summer are examined in Fig. 4. Since isoprene
261 measurements are unavailable in DT, we only analyze observations in XJH here. It
262 should be noted that the values of isoprene concentrations during summertime could
263 be larger than those displayed in Fig. 4, since the isoprene measurements were only
264 available in the morning hours (6–8 a.m.).

265 In Fig. 4a, the observed isoprene concentrations exhibited distinct seasonal
266 variations in XJH, with maximum of 0.12 ppb in summer. Zhang et al. (2012) reported
267 that observed isoprene concentrations also showed remarkable diurnal variations in
268 Shanghai, suggesting that the observed isoprene in Shanghai mainly came from
269 biogenic sources. According to the government report
270 (http://www.shanghai.gov.cn/nw2/nw2314/nw3766/nw3826/nw20410/u1aw463.html),
271 the vegetation coverage in Shanghai greatly increased in past years, which could be
272 major sources of the BVOCs. Isoprene emissions are expected to change largely
273 follows the case of biogenic emissions which increase exponentially with temperature
274 until approximately 40°C and then decrease due to the biophysical high-temperature
275 constrains (Guenther et al., 1993; Di Carlo et al., 2004). In Fig. 4b, observed isoprene
276 concentrations in XJH showed significant increases as temperature went up in
277 summer, with an average increasing rate of 0.01 ppb $°C^{-1}$. Since urban Shanghai is

VOC-sensitive, the temperature-dependent increases in isoprene emissions could contribute to the increases in O_3 at warmer temperature.

Fig. 4a also shows the observed seasonal variations of $NO_{x\text{-}max}$ in XJH. Observed seasonal mean $NO_{x\text{-}max}$ concentrations exhibited lowest values in summer as a result of the higher photo-activity, relatively deep PBLH and dilution effects of the prevailing winds (Geng et al., 2008). In Fig. 4b, summertime $NO_{x\text{-}max}$ concentrations slightly increased as temperature became warmer, with an average increasing rate of 1.01 ppb $°C^{-1}$. Early studies suggested that the increase in summertime NO_x could be attributed to the enhancement of PAN decomposition (Sillman and Samson, 1995; Steiner et al., 2010). As temperature increases, more NO_x are released which tends to remove more OH radicals from the active VOC oxidation cycle, and then retard the production of O_3 (Seinfeld and Pandis, 2006). Emissions of NO_x and VOCs from anthropogenic sources might also increase at warmer temperatures due to rises in energy demand and evaporative emission in summer (Steiner et al., 2010). However, there are large uncertainties in the relationships between anthropogenic emissions and warmer temperatures (Rubin et al., 2006; Steiner et al., 2010). Observed $NO_{x\text{-}max}$ concentrations still exhibit lowest values in summer, suggesting that the temperature-related changes in anthropogenic emissions could not be dominant in influencing NO_x concentrations.

Meteorological conditions (Chang et al., 2019, Li et al., 2019b) may also affect the $m_{O3\text{-}T}$. In summer, high temperature is usually related to changes in convective precipitation, winds and even the subtropical high control type weather in Shanghai,

300 which influence O_3 production. We shown the observed summertime O_3-temperature
301 relationships during rainless days and days with lower wind speeds in the two sites of
302 Shanghai in Fig. 5. However, the differences between $m_{O3\text{-}T}$ values in different days
303 were quite small, suggesting small influence of precipitation and wind on the climate
304 penalty in Shanghai. The observed mean values of T_{max} in XJH and DT are 33.0 °C
305 and 29.3 °C, respectively in summer during time period 2010–2017. However, The
306 rural site (DT) with low T_{max} and high isoprene emissions has much larger $m_{O3\text{-}T}$
307 values than the urban site with high T_{max} and low isoprene emissions (Fig. 3). As such ,
308 the result indicates that $m_{O3\text{-}T}$ should be mainly driven by temperature-dependent
309 emissions through atmospheric chemistry and ecosystem-climate interactions rather
310 than the temperature-induced meteorological conditions.

311 **3.3.2 Modeled sensitivity of $m_{O3\text{-}T}$ to emissions**

312 To further examine the role of precursors in determining $m_{O3\text{-}T}$ during summertime,
313 sensitivity experiments are performed using the NCAR Master Mechanism model in
314 Shanghai. Separate simulations are conducted under different emission scenarios in
315 XJH and DT, respectively. The basic diurnal variations of temperature in XJH and DT
316 are assigned according to the observed mean values in summer during time period
317 2010–2017 (Fig. S3). The diurnal variations for each temperature bin are assigned by
318 increasing/decreasing multiples of 2°C based on the basic diurnal variations, with
319 daily maximum temperature ranging from 19–43°C. To obtain a stable state in the
320 simulations, the photochemistry for O_3 is calculated for a 2-day period for each station,
321 and model results of the last day are used to explore the roles of precursor emissions

in O_3 formation of Shanghai. The detailed descriptions of the experiments are in the following:

(1) BASE case: Simulation with basic anthropogenic emissions and fixed biogenic isoprene emissions scaled to the basic temperature.

(2) ISOP case: Same as BASE but with a temperature-dependent change in biogenic isoprene emissions for each temperature bin. The emission rates are derived based on the isoprene-temperature parameterization of Guenther et al. (2006) (Fig. S2).

(3) AVOC case: Same as BASE but with a temperature-dependent change in anthropogenic VOC (AVOC) emissions for each temperature bin. The emission rates increase 1% per 3 °C according to Steiner et al. (2010).

(4) NO_x case: Same as BASE but with a temperature-dependent change in NO_x emissions for each temperature bin. The emission rates increase 1% per 3 °C, similar as AVOC emissions.

Fig. 6 exhibits the calculated relationships between $O_{3\text{-}max}$ and T_{max} in different cases for XJH and DT. In the BASE case, the modeled changes in $O_{3\text{-}max}$ with T_{max} are only attributed to the impact of temperature on chemical reactions since emissions remain unchanged in simulations conducted for each temperature bin. The simulated BASE case O_3 increases slower as temperature goes up in XJH, and the result can be well explained by the temperature-induced acceleration of PAN decomposition. Fig. 7a displays the relationship of daily maximum PAN with the increasing temperature in the BASE case simulations. Simulated PAN concentration

exhibits an apparent decline as temperature becomes warmer in both urban and rural sites. Reaction rate for (NO_2+OH→HNO_3) could be expressed as k[NO_2][OH], where k is the rate consistent calculated according to the temperature. As displayed in Fig. 7b, the values of k[NO_2][OH] increase as temperature goes up in both sites, indicating that more OH radicals could be removed by NO_x with current VOCs/NO_x ratios, hindering the production of O_3. The magnitudes of the simulated PAN and k[NO_2][OH] are comparable to those reported in previous studies (Sillman and Samson, 1995; Lin et al., 2009).

Fig. 6 also displays the model results from the ISOP, AVOC and NO_x cases, which reflect the changes in $m_{O3\text{-}T}$ depending on the degree of VOC or NO_x emissions. In the ISOP case, $m_{O3\text{-}T}$ in both sites exhibit most significant changes as the temperature increases. The simulated O_3 concentrations grow faster as temperature goes up, and show decreasing changes at approximately 40°C when the isoprene emissions begin to decrease. The pattern is similar to the observed summertime O_3-temperature relationships (Fig. 3), though decreases in O_3 at extremely high temperature don't appear in the observational results due to the limited measurements. In spite of low anthropogenic emissions, both the observational and model results suggest that O_3 concentrations in DT increase faster than those in XJH since the isoprene emissions in DT are much higher and more sensitive to the increasing temperature (Fig. 6b). From this point of view, the temperature dependence of biogenic isoprene emissions could be very important in determining the observed responses of O_3 to the increasing temperature.

Model results from the AVOC and NO_x case simulations indicate that only considering the temperature-related changes in AVOC and NO_x emissions cannot bring out the observed increases in O_3 as temperature goes up (Fig. 6). In the AVOC case, increases in AVOC emissions promote the increases in O_3 as temperature goes up in XJH as well; however, the effects are much smaller than those of the isoprene emissions. Since XJH is strongly VOC-sensitive, model result from the NO_x case exhibits a decrease in both O_3 concentrations and $m_{O3\text{-}T}$ at high temperature due to the increases in NO_x emissions. DT is less VOC-sensitive and has fairly low anthropogenic emissions, thus the impacts of AVOC and NO_x emissions are both inconspicuous.

It should be noted that values of modeled $O_{3\text{-}max}$ and $m_{O3\text{-}T}$ differs from observed values (Fig. 3 and Fig. 6). Similar mismatch has been noted in previous studies (e.g. Steiner et al., 2010) indicating the roles of meteorological characteristics (e.g. stagnation and transport) that are not considered in box model except for uncertainties in emissions and initial conditions. In real atmosphere, for example, long-distance transport of pollutants can be also important in O_3 formation, especially in rural site with low anthropogenic emissions like DT. Transport of air mass and aged pollutants from the urban region might further influence changes in $m_{O3\text{-}T}$ in rural sites as temperature becomes warmer.

3.4 Effect of emission reductions on $m_{O3\text{-}T}$

The increasing severity of O_3 pollution in Chiness megacities raises a new challenge to current emission control policies. To evaluate the response of $m_{O3\text{-}T}$ to emission

388 reductions, we examine the variations of m_{O3-T} during time period 2010–2017 and
389 discuss the possible changes under future emission control actions in this section
390 based on observations as well as numerical experiments.

391 According to the observed O_3 exceedance and NO_x concentrations in Figs. 1–2,
392 we divide the period of 2010–2017 into two parts: Period 1 (2010–2012) with less O_3
393 exceedance days and higher NO_x concentrations, and Period 2 (2013–2017) with
394 more O_3 exceedance days and lower NO_x concentrations. Fig 8a–b display the
395 observed summertime O_3-temperature relationships during Period 1 and Period 2 in
396 XJH and DT, respectively. In urban site (XJH), the mean value of m_{O3-T} increased
397 from 1.52 ppb $°C^{-1}$ in Period 1 to 2.97 ppb $°C^{-1}$ in Period 2, suggesting that the
398 reductions in NO_x emissions might strengthen the high-temperature O_3 response in
399 urban Shanghai. The observed mean m_{O3-T} value in DT slightly increased from 4.46
400 ppb$°C^{-1}$ in Period 1 to 5.05 ppb $°C^{-1}$ in Period 2, the increase of which were smaller
401 than that in XJH. Since DT exhibited a little NO_x-sensitive as discussed in Sec. 3.1,
402 the changes might result from the slightly increases in NO_x concentrations during the
403 two periods. According to the observational results, the m_{O3-T} in urban Shanghai are
404 more sensitive to the changes in anthropogenic emissions and could be aggravated
405 by the current NO_x reduction actions.

406 Numerical experiments are performed to further examine the response of m_{O3-T} to
407 various emission reduction measures. As discussed in Sec. 3.3, the temperature
408 dependence of biogenic isoprene emissions could be the key driver of the observed
409 responses of O_3 to the increasing temperature in Shanghai. Therefore, we conducted

the following sensitivity experiments to evaluate the effect of different emission reductions on the O_3-temperature relationship. Similar to the experiments in Sec. 3.3.2, the second day calculations from the 2-day simulations are used for the analyses.

(1) EMI_2010: Same as ISOP case in Sec.3.3.2, with anthropogenic emissions based on MEIC inventory for year 2010.

(2) EMI_2017: Same as EMI_2010 but with a 30% reduction in NO_x emissions. The reductions are obtained from comparisons between MEIC inventories for the year 2010 and 2017 (Zheng et al., 2018).

(3) EMI_202xA: Same as EMI_2017 but with a 15% reduction in NO_x emissions.

(4) EMI_202xB: Same as EMI_2017 but with a 15% reduction in anthropogenic VOC emissions.

Figs. 8c–d exhibit the calculated O_3-temperature relationships from various sensitivity experiments. For the rural site (DT), the local emission reductions have little influence on O_3 concentrations and $m_{O3\text{-}T}$ since the anthropogenic emissions are quite low. For the urban site (XJH), decreases in NO_x emissions result in increases in O_3 concentrations, while decreases in AVOC emissions lead to reductions in O_3 concentrations. The calculated mean values of $m_{O3\text{-}T}$ in XJH are 1.35 and 2.00 ppb $°C^{-1}$ in EMI_2010 and EMI_2017 simulations, respectively, suggesting that NO_x emission reductions can greatly increase the response of O_3 to the increasing temperatures at present. If the NO_x emissions continue to decrease following the EMI_202xA case, O_3 concentrations would increase further. However, as NO_x

emissions decreases, the O_3 production in urban Shanghai would convert from the VOC-sensitive regime to the transitional regime. As such, the sensitivity of $m_{O3\text{-}T}$ to the BVOC emissions might be weakened, resulting in slight decrease in $m_{O3\text{-}T}$ in the EMI_202xA (1.83 ppb $°C^{-1}$) compared to that in EMI_2017. For the substantial emissions and complex sources, VOC emission reduction actions have just started in China recently (http://www.gov.cn/zhengce/content/2018-07/03/content_5303158.htm). As reported in Gao et al. (2017), the VOC concentrations in urban Shanghai were relatively unchanged during past years. However, in the next few years, the VOC emission reductions would influence the O_3 formation in China with the advancing of the emission control policies. In the EMI_202xB case, the calculated mean value of $m_{O3\text{-}T}$ decreases to 1.63 ppb $°C^{-1}$ in XJH compared to that in EMI_2017, indicating that reductions in AVOC emissions would not only relieve the O_3 pollution, but also decrease the high-temperature O_3 response in megacities like Shanghai.

4. Conclusions and Discussion

Surface O_3 pollution in Shanghai worsened during time period 2010–2017, with the numbers of O_3 exceedance days increased by 8.3 and 1.3 times in urban (XJH) and rural (DT) sites, respectively. The observed $O_{3\text{-}max}$ and NO_{max} ($NO_{2\text{-}max}$) were strongly anti-correlated in XJH from 2010 to 2017, indicating a strong depression of NO_x on O_3 at urban site. Based on observational data, the ozone-climate penalty, defined as the slope of the O_3-temperature relationship ($m_{O3\text{-}T}$), was examined in Shanghai over the period 2010–2017. Statistical results show that the response of O_3 on the temperature increases was most significant in summer, with mean $m_{O3\text{-}T}$ values of

454 6.65 and 13.68 ppb $°C^{-1}$ above 30°C in XJH and DT, respectively. Different with
455 observational result in NO_x-limited sites in previous studies (Sillman and Samson,
456 1995; Jing et al., 2017), the rural site (DT) with lower NO_x emissions had steeper
457 $m_{O3\text{-}T}$ than the urban site (XJH) during summertime in Shanghai, indicating that local
458 VOC/NO_x ratios greatly influence the ozone-climate penalty effect.

459 The dominant drivers in determining $m_{O3\text{-}T}$ of Shanghai are evaluated based on
460 measurements and numerical experiments. The observed summertime isoprene
461 concentrations in XJH exhibited remarkable diurnal and seasonal variations in urban
462 Shanghai, and showed significant increase as temperature went up, with mean rate
463 of 0.01 ppb $°C^{-1}$ in summer. The observational results suggest that the isoprene
464 emissions are mainly biogenic. The simulated $m_{O3\text{-}T}$ values in Shanghai show strong
465 sensitivities to the temperature-induced changes in the biogenic isoprene emissions,
466 while the impact of increasing temperature on chemical reactions cannot well explain
467 the observed increases in O_3. Higher isoprene emissions in DT result in larger $m_{O3\text{-}T}$
468 values in spite of low anthropogenic emissions. The VOCs and NO_x from
469 anthropogenic sources may increase at warmer temperatures, but their influence is
470 minor. Though the high temperature-related meteorological features could amplify the
471 O_3 increase in summer, the influence of which on $m_{O3\text{-}T}$ should be inferior to that of
472 the biogenic factor in Shanghai. As a result, we conclude that the main driver of $m_{O3\text{-}T}$
473 in Shanghai is the temperature-related behaviors of BVOC emissions through
474 ecosystem-climate interactions.

475 In this study, we just examine the roles of isoprene for the limited observations. It

should be noted that although isoprene is the largest BVOC species accounting for ~40% of the total BVOC emissions in Shanghai (Liu et al., 2018), other BVOC species (e.g., monoterpene) can be greatly influenced by the temperatures. According to the Shanghai Master Plan (2017–2035) (http://www.shanghai.gov.cn/nw2/nw2314/nw32419/nw42806/), the vegetated area in Shanghai will continue to expand and will increase by a factor of 1.5 in 2035 compared to that in 2015. The urban afforestation measures will further promote the emissions of the biogenic sources and then affect the O_3 response to the increasing temperatures in Shanghai.

Climate change will increase the surface O_3 concentrations and the frequency of high O_3 episodes, implying a more significant ozone-climate penalty effect that can be mainly attributed to climate-induced increases in biogenic emissions of VOCs over East China (Lin et al., 2008; Wang et al., 2013). The calculated 2000–2050 changes in summertime temperature could be 0.8–1.5 °C in the Shanghai area. As a result of warmer temperature and stonger solar radiation, the 2000–2050 climate change would result in a 34% increase in isoprene emissions in China, and lead to a 8% increase in the sensitivity of surface O_3 to a given change in anthropogenic emissions in East China (Wang et al., 2013). The warming climate requires more aggressive emission controls to wrestle with the challenges for future O_3 pollution.

Emission reduction actions greatly influence the dependence of O_3 on increasing temperatures in Shanghai. NO_x emission reductions could strengthen the high-temperature O_3 response in urban Shanghai at present. NO_x emissions will

498 continue to decrease as require by recent governmtal Clear Air Action (Li et al.,
499 2019a), the O_3 production in urban Shanghai tend to convert to the transitional regime
500 and the sensitivity of $m_{O3\text{-}T}$ to the temperature-related BVOC changes might be
501 weakened. AVOC emission control measures would effectively relieve O_3 pollution
502 and reduce the high-temperature O_3 response in urban Shanghai. Therefore, to
503 effectively control O_3 pollution towards a warmer climate, strict emission reductions
504 as well as scientific city planning strategies are needed to balance the VOC/NO_x
505 ratios in Shanghai.

506

507 **Acknowledgments:** This work was sponsored by the National Key R&D Program of
508 China (Grant No. 2016YFC0201900), Shanghai Sailing Program (Grant No.
509 18YF1421200), the National Natural Science Foundation of China (Grant No.
510 91644223 and 41801367).

511 **References**

512 Bloomfield, P., Royle, J.A., Steinberg, L.J., Yang, Q., 1996. Accounting for
513 meteorological effects in measuring urban ozone levels and trends. Atmos.
514 Environ. 30, 3067–3077.
515 Bloomer, B.J., Stehr, J.W., Piety, C.A., Salawitch, R.J., Dickerson, R.R., 2009.
516 Observed relationships of ozone air pollution with temperature and emissions.
517 Geophys. Res. Lett. 36, 9, 269–277.
518 Chang, L. Xu, J., Qu, Y., Mao, Z., and Zhou, G., 2019. Study on objective synoptic
519 classification on ozone pollution in Shanghai. Acta Scientiae Circumstantiae,
520 39, 1, 169–179.
521 Di Carlo, P., Brune, W.H., Martinez, M., Harder, H., Lesher, R., Ren, X.R., Thornberry,

T., Carroll, M.A., Young, V., Shepson, P.B., Riemer, D., Apel, E., Campbell, C., 2004. Missing OH reactivity in a forest: evidence for unknown reactive biogenic VOCs. Science 304, 5671, 722–725.

Feng, Z.Z., De Marco, A., Anav, A., Gualtieri, M., Sicard, P., Tian, H.Q., Fornasier, F., Tao, F.L., Guo, A.H., Paoletti, E., 2019. Economic losses due to ozone impacts on human health, forest productivity and crop yield across China. Environ. Int. 131, 104966.

Fu, T.M., Zheng, Y., Paulot, F., Mao, J., Yantosca, R.M., 2015. Positive but variable sensitivity of August surface ozone to large-scale warming in the southeast United States. Nat. Clim. Change 5, 454–458.

Gao, W., Tie, X., Xu, J., Huang, R., Mao, X., Zhou, G., Chang, L., 2017. Long-term trend of O_3, in a mega city (Shanghai), China: Characteristics, causes, and interactions with precursors. Sci. Total Environ. 603–604, 425–433.

Geng, F., Qiang, Z., Tie, X., Huang, M., Ma, X., Deng, Z., Quan, J., Zhao, C., 2009. Aircraft measurements of O_3, NO_x, CO, VOCs, and SO_2 in the Yangtze River Delta region. Atmos. Environ. 43, 584–593.

Geng, F., Tie, X., Xu, J., Zhou, G., Peng, L., Gao, W., Tang, X., Zhao, C., 2008. Characterizations of ozone, NO_x, and VOCs measured in Shanghai, China. Atmos. Environ. 42, 6873–6883.

Geng, F., Zhao, C., Tang, X., Lu, G., Tie, X., 2007. Analysis of ozone and VOCs measured in Shanghai: a case study. Atmos. Environ. 41, 5, 989–1001.

Gilbert, R.O., 1987. Statistical Methods for Environmental Pollution Monitoring. John Wiley & Sons, New York.

Gocic, M., Trajkovic, S., 2013. Analysis of changes in meteorological variables using Mann-Kendall and Sen's slope estimator statistical tests in Serbia. Global Planet. Change 100, 172–182

Guenther, A., Karl, T., Harley, P., Wiedinmyer, C., Palmer, P.I., Geron, C., 2006. Estimates of global terrestrial isoprene emissions using MEGAN (model of emissions of gases and aerosols from nature). Atmos. Chem. Phys., 6(11), 3181–321.

552 Guenther, A.B., Zimmerman, P.R., Harley, P.C., Monson, R.K., Fall, R., 1993.
553 Isoprene and monoterpene emission rate variability—Model evaluations and
554 sensitivity analyses. J Geophys Res-Atmos. 98, D7, 12609–12617.
555 Jacob, D.J., Logan, J.A., Yevich, R.M., Gardner, G.M., Spivakovsky, C.M., Wofsy,
556 S.C., Munger, J.W., Sillman, S., Prather, M.J., Rodgers, M.O., Westberg, H.,
557 Zimmerman, P.R., 1993. Simulation of summertime ozone over North
558 America. J. Geophys. Res. -Atmos. 98, D8, 14797–14816.
559 Jacob, D.J., Winner, D.A., 2009. Effect of climate change on air quality. Atmos.
560 Environ. 43, 51–63.
561 Jing, P., Lu, Z., Steiner, A.L., 2017. The ozone-climate penalty in the Midwestern U.S.
562 Atmos. Environ. 170, 130–142.
563 Kendall, M.G. 1975. Rank Correlation Methods, 4th edition, Charles Griffin, London.
564 Li, M., Zhang, Q., Streets, D., He, K.B., Cheng, Y.F., Emmons, L.K., Huo, H., Kang,
565 S.C., Lu, Z., Shao, M., Su, H., Yu, X., Zhang, Y., 2014. Mapping Asian
566 anthropogenic emissions of non-methane volatile organic compounds to
567 multiple chemical mechanisms. Atmos. Chem. Phys. 14, 5617–5638.
568 Li, K., Jacob, D.J., Liao, H., Zhu, J., Shah, V., Shen, L., Bates, K.H., Zhang, Q., Zhai,
569 S., 2019a. A two-pollutant strategy for improving ozone and particulate air
570 quality in China. Nat. Geosci. https://doi.org/10.1038/s41561-019-0464-x.
571 Li, K., Jacob, D.J., Liao, H., Shen, L., Zhang, Q., Bates, K.H., 2019b. Anthropogenic
572 drivers of 2013–2017 trends in summer surface ozone in China. P. Natl. A.
573 Sci. USA 116, 2, 422–427.
574 Liao, H., Chen, W.-T., Seinfeld, J.H., 2006. Role of climate change in global
575 predictions of future tropospheric ozone and aerosols. J. Geophys. Res. 111,
576 D12304.
577 Lin, J.-T., Patien, K.O., Hayhoe, K., Liang, X., Wuebbles, D.J., 2008. Effects of Future
578 Climate and Biogenic Emissions Changes on Surface Ozone over the United
579 States and China. J. Appl. Meteorol. Clim. 47, 1888–1909.
580 Lin, M., Holloway, T., Oki, T., Streets, D.G., Richter, A., 2009. Multi-scale model
581 analysis of boundary layer ozone over East Asia. Atmos. Chem. Phys. 9,

582 3277–3301.
583 Lu, X., Hong, J., Zhang, L., Cooper, O.R., Schults, M.G., Xu, X., Wang, T., Gao, M.,
584 Zhao, Y., Zhang Y., 2018. Severe surface ozone pollution in China: A global
585 perspective. Environ. Sci. Technol. Lett. 5, 8, 487–194.
586 Liu, Y., Li, L., An, J., Huang, L., Yan, R., Huang, C., Wang, H., Wang, Q., Wang, M.,
587 Zhang, W., 2018. Estimation of biogenic VOC emissions and its impact on
588 ozone formation over the Yangtze River Delta region, China. Atmos. Environ.
589 186, 113–128.
590 Madronich, S., Flocke, S., 1999. The role of solar radiation in atmospheric chemistry.
591 In: Boule, P. (Ed.), Handbook of Environmental Chemistry. Springer-Verlag,
592 Heidelberg, pp. 1–26.
593 Madronich, S., Calvert, J.G., 1990. Permutation reactions of organic peroxy radicals
594 in the troposphere. J. Geophys. Res., 95, 5697–5715.
595 Mann, H.B. 1945. Non-parametric tests against trend, Econometrica 13, 163–171.
596 Paoletti, E., De Marco, A., Beddows, D.C.S., Harrison, R.M., Manning, W.J., 2014.
597 Ozone levels in European and USA cities are increasing more than at rural
598 sites, while peak values are decreasing. Environ. Pollut. 192, 295–299.
599 Pusede, S.E., Steiner, A.L., Cohen, R.C., 2015. Temperature and recent trends in the
600 chemistry of continental surface ozone. Chem. Rev. 115, 10, 3898–3918.
601 Pusede, S.E., Gentner, D.R., Wooldridge, P.J., Browne, E.C., Rollins, A.W., Min, K.-E.,
602 Russell, A.R., Thomas, J., Zhang, L., Brune, W.H., Henry, S.B., DiGangi, J.P.,
603 Keutsch, F.N., Harrold, S.A., Thornton, J.A., Beaver, M.R., St Clair, J.M.,
604 Wennberg, P.O., Sanders, J., Ren, X., VandenBoer, T.C., Markovic, M.Z.,
605 Guha, A., Weber, R., Goldstein, A.H., Cohen, R.C., 2014. On the temperature
606 dependence of organic reactivity, nitrogen oxides, ozone production, and the
607 impact of emission controls in San Joaquin Valley, California. Atmos. Chem.
608 Phys. 14, 3373–3395.
609 Ran, L., Zhao, C., Geng, F., Tie, X., Tang, X., Peng, L., Zhou, G., Yu, Q., Xu, J.,
610 Guenther, A., 2009. Ozone photochemical production in urban Shanghai,
611 China: Analysis based on ground level observations, J. Geophys. Res., 114,

612 D15301, doi:10.1029/2008JD010752.
613 Rasmussen, D.J. , Fiore, A.M. , Naik, V. , Horowitz, L.W. , Mcginnis, S.J. , Schultz,
614 M.G., 2012. Surface ozone-temperature relationships in the eastern U.S.: a
615 monthly climatology for evaluating chemistry-climate models. Atmos. Environ.
616 47, 142–153.
617 Rubin, J.I., Kean, A.J., Harley, R.A., Millet, D.B., Goldstein, A.H., 2006. Temperature
618 dependence of volatile organic compound evaporative emissions from motor
619 vehicles. J. Geophys. Res., 111, D03305.
620 Seinfeld, J.H. Pandis, S.N., 2006. Atmospheric chemistry and physics: From air
621 pollution to climate change, 2nd ed.; John Wiley: A Wiley-Interscience
622 Publication Press, New York, USA, pp.43–46.
623 Sen, P.K., 1968. Estimates of the regression coefficient based on Kendall's tau. J. Am.
624 Stat. Assoc. 63, 1379–1389.
625 Shan, W., Zhang, J., Huang, Z., You, L., 2010. Characterizations of ozone and related
626 compounds under the influence of maritime and continental winds at a
627 coastal site in the Yangtze Delta, nearby Shanghai. Atmos. Res., 97, 26–34.
628 Shan, W., Yang, P., Lu, H., Ma, K., Huang, Z., 2016. Influence of Coastal Wind on
629 Surface Ozone and Nitrogen Oxides in Suburban Shanghai. Asia-Pac. J.
630 Atmos. Sci., 52(5), 451–458.
631 Shen, L., Mickley, L.J., Gilleland, E., 2016. Impact of increasing heat waves on U.S.
632 ozone episodes in the 2050s: Results from a multimodel analysis using
633 extreme value theory. Geophys. Res. Lett. 43, 4017–4025.
634 Shi, C.Z., Wang, S., Liu, R., Zhou, R., Li, D., Wang, W., Li, Z., Cheng, T., Zhou, B.,
635 2015. A study of aerosol optical properties during ozone pollution episodes in
636 2013 over Shanghai, China. Atmos. Res., 153, 235–249.
637 Sicard, P., Augustaitis, A., Belyazid, S., Calfapietra, C., De Marco, A., Fenn, M.,
638 Bytnerowicz, A., Grulke, N., He, S., Matyssek, R., Serengil, Y., Wieser, G.,
639 Paoletti, E., 2016. Global topics and novel approaches in the study of air
640 pollution, climate change and forest ecosystems. Environ. Polluti. 213, 977–
641 987.

642 Sicard, P., De Marco, A., Troussier, F., Renou, C., Vas, N., Paoletti, E., 2013.
643 Decrease in surface ozone concentrations at Mediterranean remote sites and
644 increase in the cities. Atmos. Environ. 79, 705–715.
645 Steiner, A.L., Davis, A.J., Sillman, S., Owen, R.C., Michalak, A.M., Fiore, A.M., 2010.
646 Observed suppression of ozone formation at extremely high temperatures
647 due to chemical and biophysical feedbacks. P. Natl. A. Sci. USA 107, 46,
648 19685–19690.
649 Steiner, A.L., Tonse, S., Cohen, R.C., Goldstein, A.H., Harley, R.A., 2006. Influence of
650 future climate and emissions on regional air quality in California. J. Geophys.
651 Res.-Atmos. 111, D18303, doi:10.1029/2005JD006935.
652 Sillman, S., 2003. Photochemical smog: ozone and its precursors. Handbook of
653 Weather, Climate, and Water, Potter, T. and Bradley Roy, R. Eds.; Wiley, New
654 York, USA, pp 227–242.
655 Sillman, S., Samson, F.J., 1995. Impact of temperature on oxidant photochemistry in
656 urban, polluted, rural and remote environments. J. Geophys. Res.-Atmos.,
657 100, D6, 11497–11508.
658 Tie, X., Geng, F., Guenther, A., Cao, J., Greenberg, J., Zhang, R., Apel, E., Li, G.,
659 Weinheimer, A., Chen, J., Cai, C., 2013. Megacity impacts on regional ozone
660 formation: observations and WRF-Chem modeling for the MIRAGE-Shanghai
661 field campaign. Atmos. Chem. Phys. 13, 5655–5669.
662 Tie, X., Geng, F., Peng, L., Gao, W., Zhao, C., 2009. Measurement and modeling of
663 O_3 variability in Shanghai, China: Application of the WRF-Chem model.
664 Atmos. Environ. 43, 4289–4302.
665 Wang, T., Xue, L., Brimblecombe, P., Lam, Y., Li, L., Zhang, L., 2017. Ozone pollution
666 in China: A review of concentrations, meteorological influences, chemical
667 precursors, and effects. Sci. Total Environ. 575, 1582–1596.
668 Wang, Y., Shen, L., Wu, S., Mickley, L., He, J., Hao, J., 2013. Sensitivity of surface
669 ozone over China to 2000–2050 global changes of climate and emissions.
670 Atmos. Environ. 75, 374–382.
671 Yue, X., Unger, N., 2014. Ozone vegetation damage effects on gross primary

productivity in the United States. Atmos. Chem. Phys. 14, 9137–9153.

Zhang, W., 2012. Research on isoprene in Shanghai, China. Master thesis, Department of Atmospheric and Oceanic Sciences, School of Physics, Peking University, China, 57pp.

Zheng, B., Tong, D., Li, M., Liu, F., Hong, C., Geng, G., Li, H., Li, X., Peng, L., Qi, J., Yan, L., Zhang, Y., Zhao, H., Zheng, Y., He, K., Zhang, Q., 2018. Trends in China's anthropogenic emissions since 2010 as the consequence of clean air actions. Atmos. Chem. Phys., 18, 14095–14111.

Zhou, G., Xu, J., Xie, Y., Chang, L., Gao, W., Gu, Y., Zhou. J., 2017. Numerical air quality forecasting over eastern China: an operational application of WRF-Chem. Atmos. Environ. 153, 94–108.

Table and Figure captions:

Table 1. Statistical results for the observed O_3–temperature relationships, $y=b_0+b_1x+b_2x^2$, in Xujiahui (XJH, urban site) and Dongtan (DT, rural site), where x is daily maximum temperature (ºC) and y is daily maximum O_3 (ppb), in Spring (March–May), Summer (June-August), autumn (September–November), and winter (December–February).

Fig. 1. Changes of O_3 exceedance (number of days with O_3 concentration exceeding the Chinese Grade II national air quality standard, defined as MDA8 >160 μg m^{-3}, unit: days yr^{-1}), $O_{3\text{-max}}$ (mean of daily maximum 1-h O_3, unit: ppb), $O_{3\text{-min}}$ (mean of daily minimum 1-h O_3, unit: ppb), mean of daily maximum temperature (T_{max}, unit: ˚C), and mean of daily minimum temperature (T_{min}, unit: ˚C) in a. Xujiahui (XJH) and b. Dongtan (DT) from 2010–2017. The Mann-Kendall trend significance and the Sen trend estimate methods were used to assess the trends of variables.The slopes of the trends and the significance level as represented by the *α* value are provided in the plots.

Fig. 2. Same as Fig. 1, but for $NO_{\text{-max}}$ (mean of daily maximum 1-h NO), $NO_{2\text{-max}}$ (mean of daily maximum 1-h NO_2), $NO_{\text{-min}}$ (mean of daily minimum 1-h NO,), and $NO_{2\text{-min}}$ (mean of daily minimum 1-h NO_2) in a. Xujiahui (XJH) and b. Dongtan (DT), respectively. The slopes of the trends and the significance level as represented by the α value are provided in the plots.

Fig. 3. Observed ozone-temperature relationships in Shanghai for the period 2010–2017. Points represent the mean of the daily maximum O_3 versus local daily

maximum surface temperature for each temperature bin in Xujiahui (XJH) and Dongtan (DT), respectively. Data are binned to 2 °C intervals, and results are shown for a. spring, b. summer, c. autumn, and d. winter.

Fig. 4. a. Observed seasonal mean variations of $NO_{x\text{-}max}$ and isoprene concentrations, and b. observed corresponding summertime relationships with temperature in Xujiahui (XJH). Since isoprene measurements are only conducted during 6 to 8 am in inconsecutive days during 2010–2015, solid points in blue color represent the diurnal 3-hour averaged isoprene concentrations versus corresponding temperature. Hollow points in red color represent the means of daily maximum NO_x concentrations versus corresponding daily maximum temperatures during 2010–2017. Data are binned same as Fig. 3.

Fig. 5. Observed summertime ozone-temperature relationships for all days, days without rain, and days with daily mean wind speeds lower than the seasonal mean wind speeds in a. Xujiahui (XJH) and b. Dongtan (DT) , respectively during 2010–2017. The seasonal mean wind speeds are 1.0 and 4.8 ms^{-1} in XJH and DT, respectively in summer. The significance level is represented by the α value in the plots.

Fig. 6 Modeled ozone–temperature relationships in a. Xujiahui (XJH) and b. Dongtan (DT) from BASE (solid square in blue), ISOP (hollow square in green), AVOC (solid circle in yellow), and NO_x (hollow circle in red) cases, respectively. Data are binned same as Fig. 3.

Fig. 7 Modeled relationships of daily maximum a. PAN and b. $k[NO_2][OH]$ with daily

maximum temperatures in the BASE case simulations in Xujiahui (XJH) and Dongtan (DT), respectively. k[NO_2][OH] is the reaction rates of (NO_2+OH→HNO_3) calculated by the NCAR Master Mechanism.

Fig. 8. Observed summertime ozone-temperature relationships in a. Xujiahui (XJH) and b. Dongtan (DT) for separate years during Period 1 (2010–2012) and Period 2 (2013–2017). Also shown is the modeled ozone–temperature relationships in c. XJH and d. DT from EMI_2010, EMI_2017, EMI_202xA, and EMI_202xB case simulations, respectively. Data are binned same as Fig. 3. The significance level as represented by the α value are also provided.

736 **Table 1**. Statistical results for the observed O_3–temperature relationships,
737 $y=b_0+b_1x+b_2x^2$, in Xujiahui (XJH, urban site) and Dongtan (DT, rural site), where x is
738 daily maximum temperature (ºC) and y is daily maximum O_3 (ppb), in Spring (March–
739 May), Summer (June-August), autumn (September–November), and winter
740 (December–February).

Site	Seasons	b_0	b_1	b_2	$b_1/(-2b_2)$	$2b_2$
XJH	Spring	37.13*	-0.46*	0.06*	3.83*	0.12*
	Summer	249.18*	-16.29*	0.31*	26.27*	0.62*
	Autumn	25.73*	-0.44*	0.05*	4.40*	0.10*
	Winter	26.65*	-0.13*	0.05*	1.30*	0.10*
DT	Spring	62.29*	-1.94*	0.13*	7.46*	0.26*
	Summer	473.50*	-33.45*	0.67*	24.96*	1.34*
	Autumn	33.10*	1.04*	0.01*	-52.00*	0.02*
	Winter	38.26	1.48	-0.05	14.80	-0.10

741 *Statistically significant values at the 5% significance level.

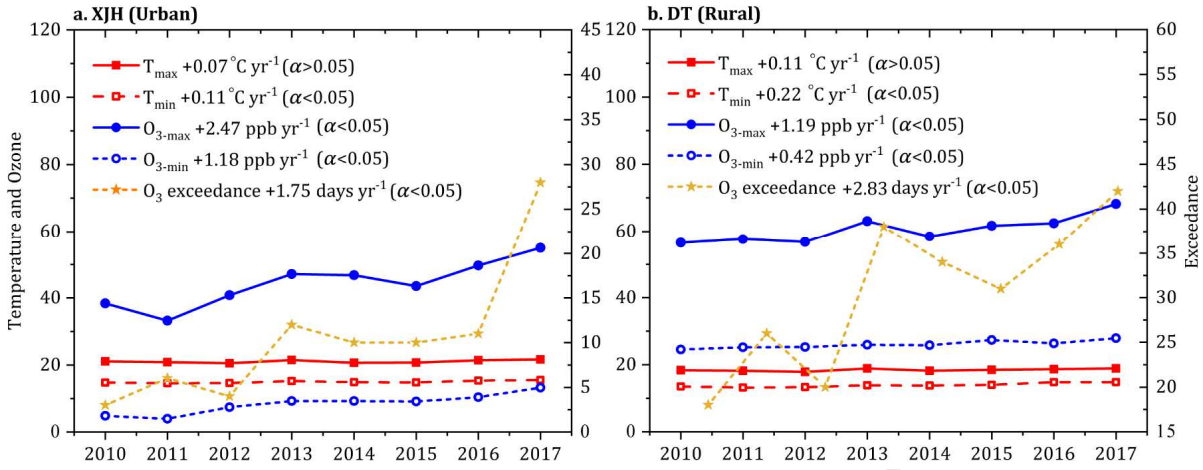

Fig. 1. Changes of O_3 exceedance (number of days with O_3 concentration exceeding the Chinese Grade II national air quality standard, defined as MDA8 >160 μg m^{-3}, unit: days yr^{-1}), $O_{3\text{-max}}$ (mean of daily maximum 1-h O_3, unit: ppb), $O_{3\text{-min}}$ (mean of daily minimum 1-h O_3, unit: ppb), mean of daily maximum temperature (T_{max}, unit: ˚C), and mean of daily minimum temperature (T_{min}, unit: ˚C) in a. Xujiahui (XJH) and b. Dongtan (DT) from 2010–2017. The Mann-Kendall trend significance and the Sen trend estimate methods were used to assess the trends of variables. The slopes of the trends and the significance level as represented by the *α* value are provided in the plots.

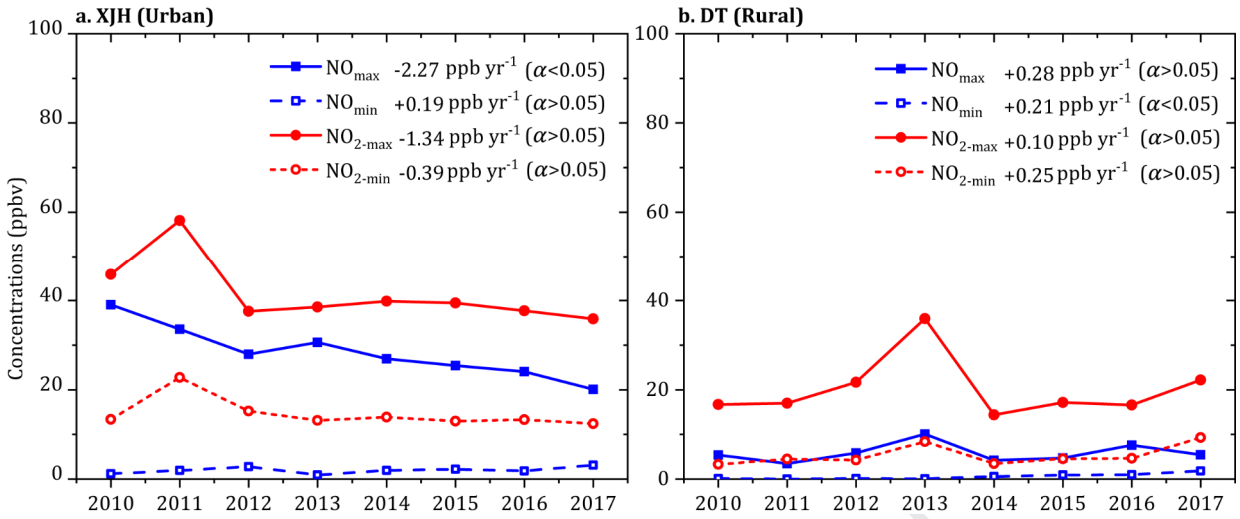

752

753 **Fig. 2.** Same as Fig. 1, but for NO_{-max} (mean of daily maximum 1-h NO), NO_{2-max}

754 (mean of daily maximum 1-h NO_2), NO_{-min} (mean of daily minimum 1-h NO,), and

755 NO_{2-min} (mean of daily minimum 1-h NO_2) in a. Xujiahui (XJH) and b. Dongtan (DT),

756 respectively. The slopes of the trends and the significance level as represented by the

757 α value are provided in the plots.

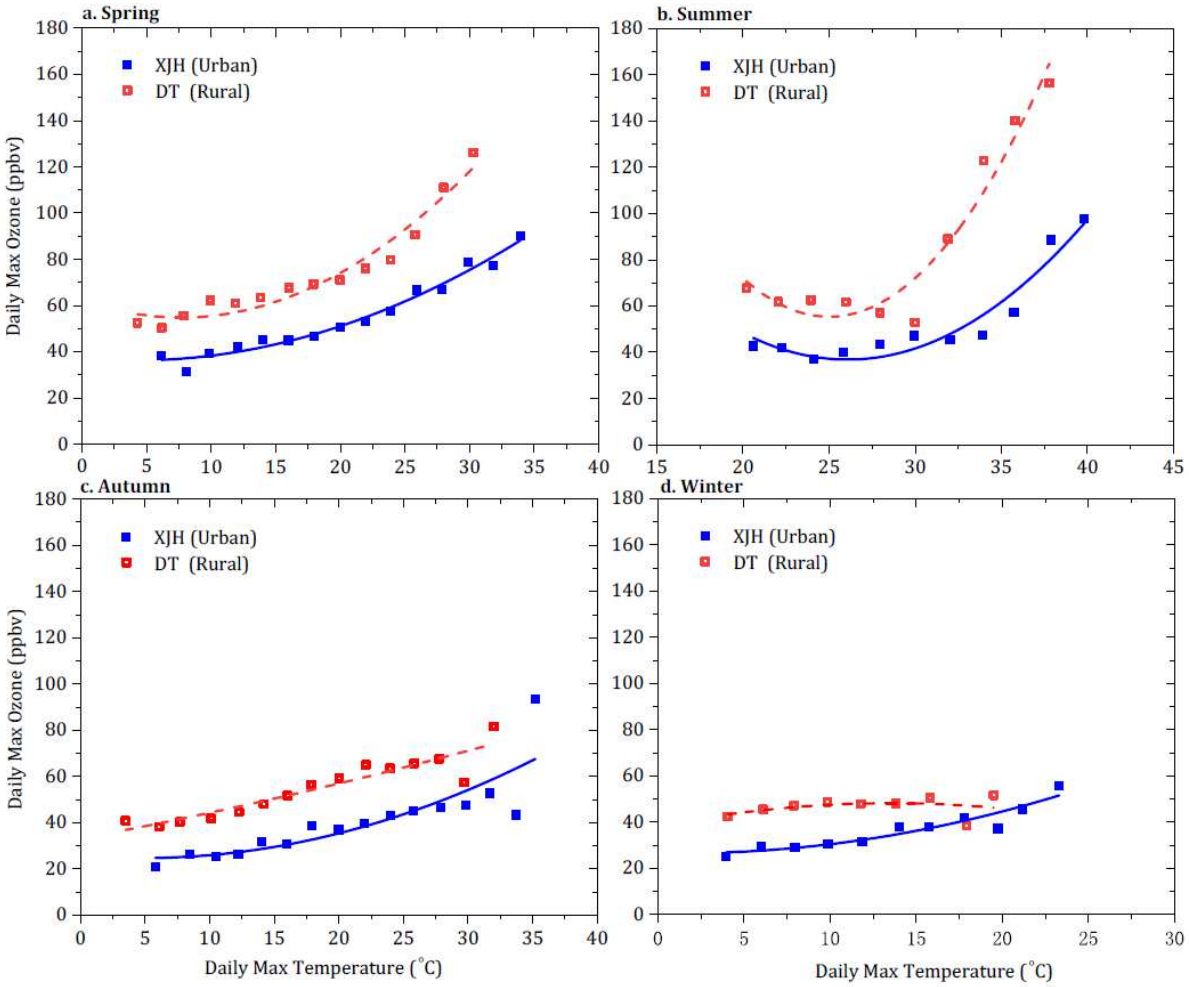

Fig. 3. Observed ozone-temperature relationships in Shanghai for the period 2010–2017. Points represent the mean of the daily maximum O_3 versus local daily maximum surface temperature for each temperature bin in Xujiahui (XJH) and Dongtan (DT), respectively. Data are binned to 2 °C intervals, and results are shown for a. spring, b. summer, c. autumn, and d. winter.

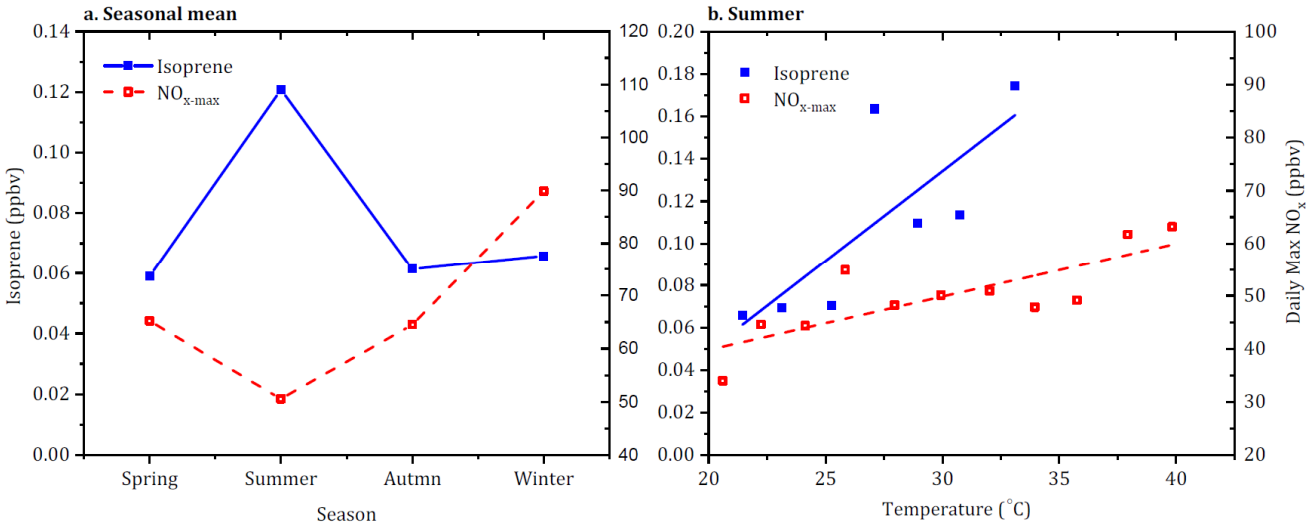

764

765 **Fig. 4.** a. Observed seasonal mean variations of $NO_{x\text{-}max}$ and isoprene concentrations,

766 and b. observed corresponding summertime relationships with temperature in

767 Xujiahui (XJH). Since isoprene measurements are only conducted during 6 to 8 am in

768 inconsecutive days during 2010–2015, solid points in blue color represent the diurnal

769 3-hour averaged isoprene concentrations versus corresponding temperature. Hollow

770 points in red color represent the means of daily maximum NO_x concentrations versus

771 corresponding daily maximum temperatures during 2010–2017. Data are binned

772 same as Fig. 3.

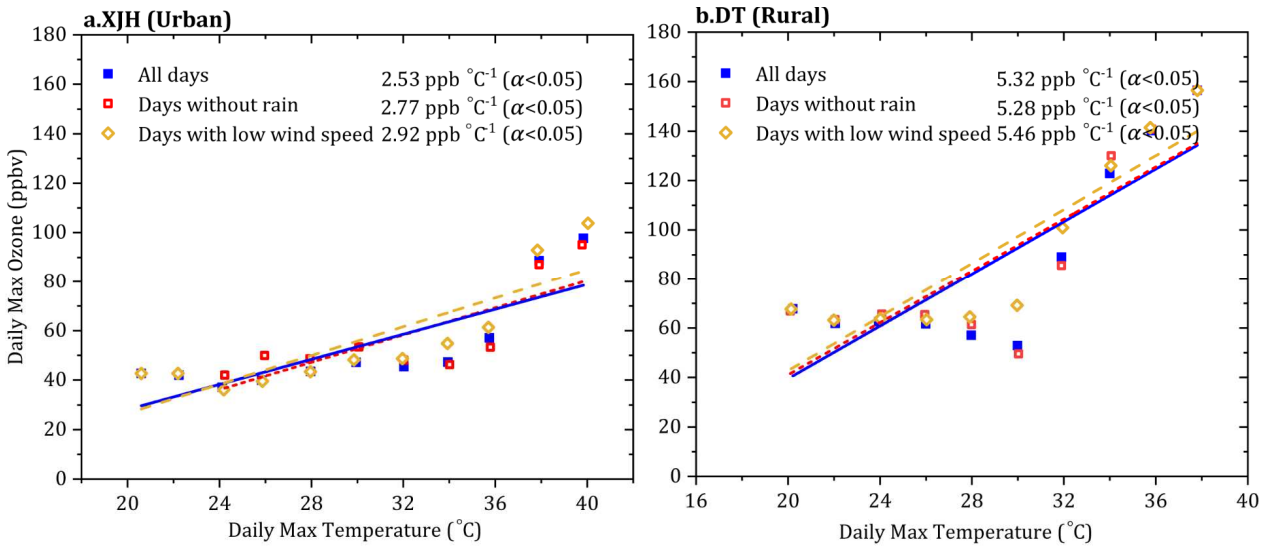

773

774 **Fig. 5.** Observed summertime ozone-temperature relationships for all days, days
775 without rain, and days with daily mean wind speeds lower than the seasonal mean
776 wind speeds in a. Xujiahui (XJH) and b. Dongtan (DT) , respectively during 2010–
777 2017. The seasonal mean wind speeds are 1.0 and 4.8 ms^{-1} in XJH and DT,
778 respectively in summer. The significance level is represented by the α value in the
779 plots.

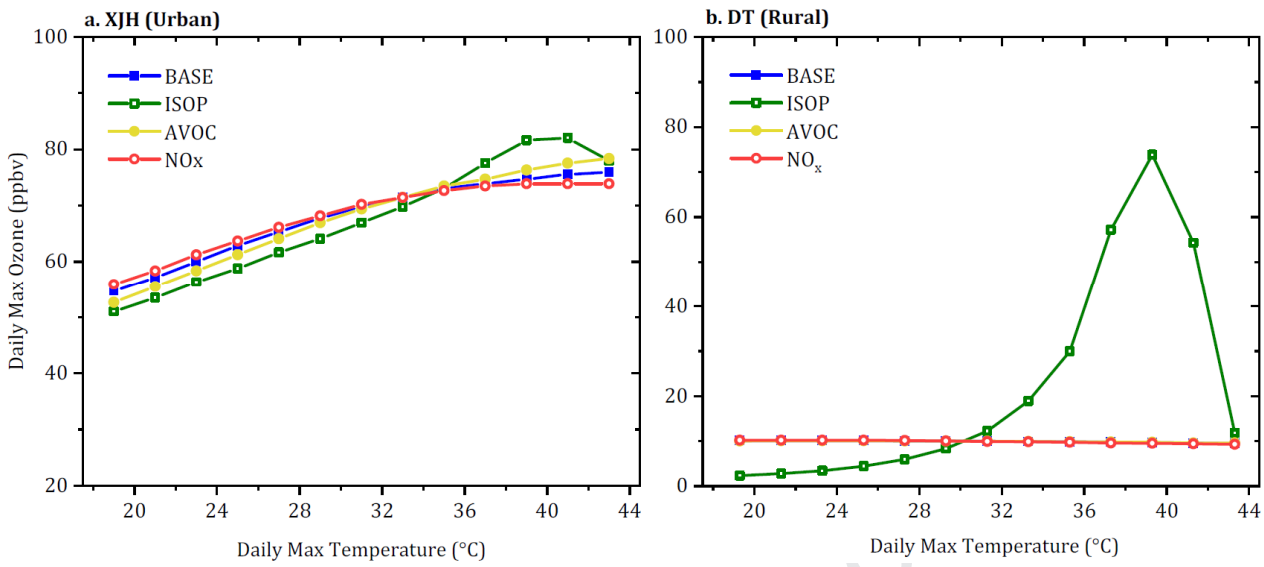

780

781 **Fig. 6** Modeled ozone–temperature relationships in a. Xujiahui (XJH) and b. Dongtan
782 (DT) from BASE (solid square in blue), ISOP (hollow square in green), AVOC (solid
783 circle in yellow), and NO_x (hollow circle in red) cases, respectively. Data are binned
784 same as Fig. 3.

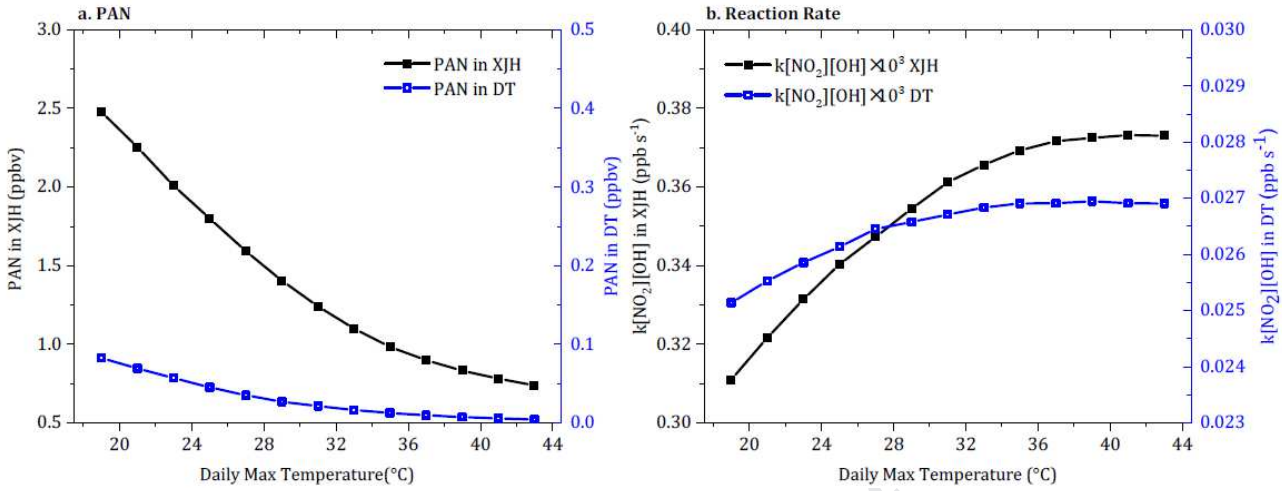

785

786 **Fig. 7** Modeled relationships of daily maximum a. PAN and b. $k[NO_2][OH]$ with daily

787 maximum temperatures in the BASE case simulations in Xujiahui (XJH) and Dongtan

788 (DT), respectively. $k[NO_2][OH]$ is the reaction rates of ($NO_2+OH \rightarrow HNO_3$) calculated

789 by the NCAR Master Mechanism.

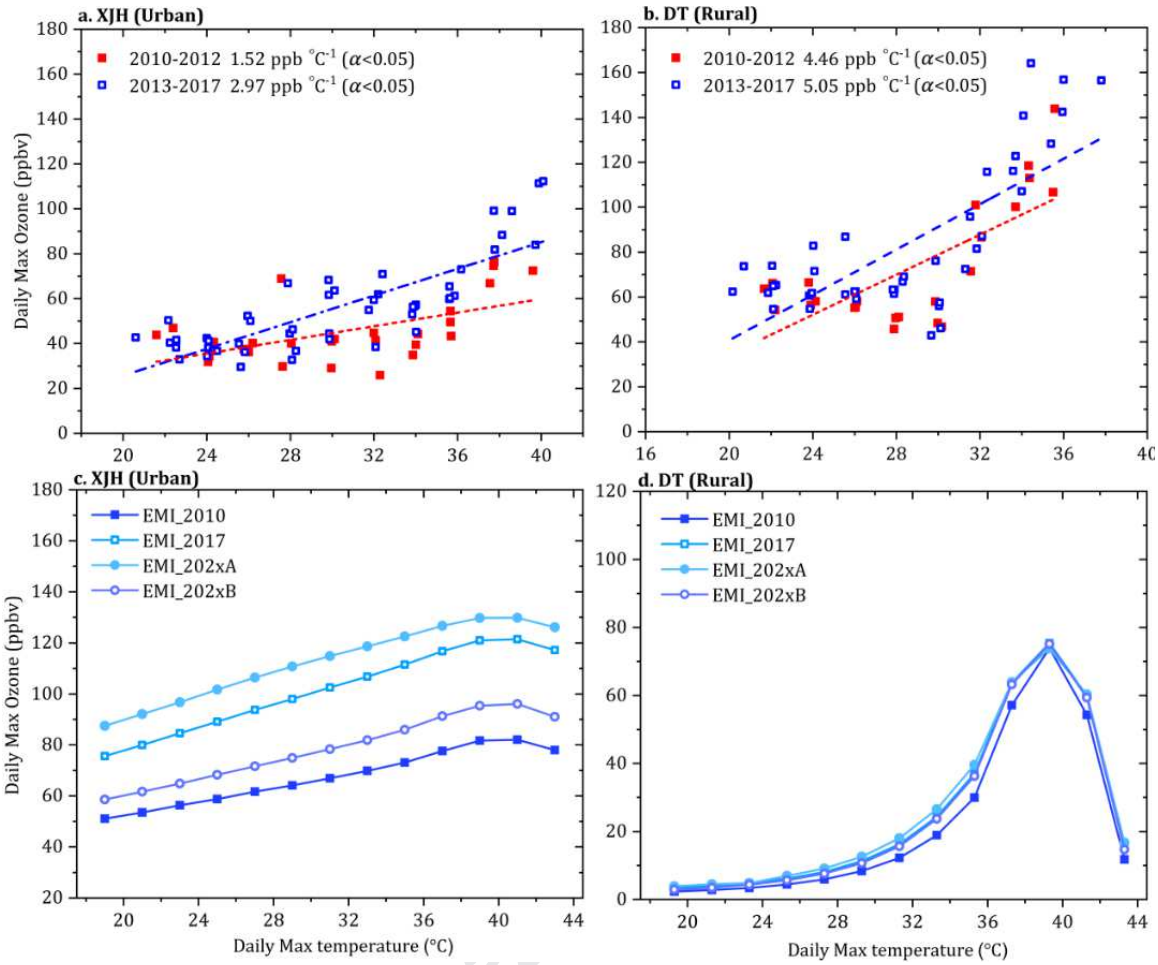

790

791 **Fig. 8.** Observed summertime ozone-temperature relationships in a. Xujiahui (XJH)

792 and b. Dongtan (DT) for separate years during Period 1 (2010–2012) and Period 2

793 (2013–2017). Also shown is the modeled ozone–temperature relationships in c. XJH

794 and d. DT from EMI_2010, EMI_2017, EMI_202xA, and EMI_202xB case simulations,

795 respectively. Data are binned same as Fig. 3. The significance level as represented

796 by the α value are also provided.

Highlights

- Surface O_3 in Shanghai increased during 2010–2017, with decreased NO_x level in urban city.
- The high-temperature O_3 response is stronger in low NO_x emission area.
- Biogenic VOCs dominate the high-temperature O_3 response in urban Shanghai.
- NO_x reductions increase the sensitivity of O_3 to increases in temperature.

Conflicts of Interest

The authors declared that they have no conflicts of interest to this work.